Chinese Chemical Letters 35 (2024) 109457

Contents lists available at ScienceDirect

Chinese Chemical Letters

journal homepage: www.elsevier.com/locate/cclet

Chlorogenic acid supported strontium polyphenol networks ensemble microneedle patch to promote diabetic wound healing

Peizhe Li[a,1], Qiaoling Liu[b,1], Mengyu Pei[d,1], Yuci Gan[a], Yan Gong[c], Chuchen Gong[a], Pei Wang[c], Mingsong Wang[c], Xiansong Wang[c,*], Da-Peng Yang[b,e], Bo Liang[b,*], Guangyu Ji[c,*]

[a] Research Institute of Plastic Surgery, Weifang Medical University, Weifang 261000, China
[b] The Second Affiliated Hospital of Fujian Medical University, Quanzhou 362000, China
[c] Department of Thoracic surgery, Shanghai Key Laboratory of Tissue Engineering, Shanghai Ninth People's Hospital, Shanghai Jiao Tong University School of Medicine, Shanghai 200011, China
[d] The Third Affiliated Hospital of Xinxiang Medical University, Institutes of Health Central Plain, Clinical Medical Center of Tissue Engineering and Regeneration, Xinxiang Medical University, Xinxiang 453003, China
[e] School of Rehabilitation Science and Engineering, University of Health and Rehabilitation Sciences, Qingdao 266024, China

ARTICLE INFO

Article history:
Received 31 October 2023
Revised 21 December 2023
Accepted 22 December 2023
Available online 26 December 2023

Keywords:
Chlorogenic acid
Strontium
Microneedle patch
Strontium polyphenol network
Exudate absorption
Diabetic wound healing

ABSTRACT

Delayed or non-healing of diabetic wounds is a significant complication, often attributed to high glucose-induced M1 macrophage accumulation, impaired angiogenesis, and reactive oxygen species (ROS) buildup. Addressing this, we introduced a strontium polyphenol network microneedle patch (SrC-MPNs@MN-PP) for percutaneous drug delivery. This patch, formulated with polymer poly(γ-glutamic acid) (γ-PGA) and epsilon-poly-L-lysine (ε-PLL), incorporates strontium polyphenol networks (SrC-MPNs). The release of chlorogenic acid (CGA) from SrC-MPNs not only neutralizes ROS, but strontium ions also foster angiogenesis. Consequently, SrC-MPNs@MN-PP can ameliorate the diabetic wound microenvironment and expedite healing.

Diabetes represents a major public health challenge due to its rising incidence and mortality rates, affecting millions globally [1,2]. Hyperglycemia in diabetics can manifest as various systemic complications; these can further evolve into a myriad of local lesions such as chronic inflammation [3], bacterial infections [4,5], dysangiogenesis [6,7], and excessive buildup of reactive oxygen species (ROS) [8,9], such complications often culminate in delayed or non-healing diabetic wounds. In extreme scenarios, this could escalate to conditions like amputation, sepsis, and can be fatal [10]. The pressing issue of non-healing diabetic wounds underscores the dire need for innovative therapeutic strategies in contemporary medical practice [11].

In treating diabetic wounds, clinicians often resort to silver ion, chitosan, and bioactive dressings. For instance, while silver ion dressings exhibit potent antibacterial efficacy *in vitro*, concerns linger regarding their potential toxicity and adverse effects in humans [12]. Chitosan dressings are noted for their safety, properties. However, the poor solubility of chitosan hampers its broader applications [13]. Some bioactive dressings, known for their anti-inflammatory and pro-regenerative traits, but it has drug resistance [14]. Our preliminary studies highlighted the efficacy and biosafety of using polymer poly(γ-glutamic acid) (γ-PGA) as a dressing combined with cell-free fat extract (CEFFE) for diabetic wound care [15]. Further innovation was achieved by converting γ-PGA into soluble microneedles (MNs), which were specifically developed for the treatment of diabetic wounds and hair regeneration. These MNs offer a controlled drug release mechanism and boast commendable mechanical strength and regenerative capabilities [16–18]. Furthermore, our research indicates that epsilon-poly-L-lysine (ε-PLL) exhibits significant antibacterial activity and biocompatibility. A novel adhesive hydrogel dressing, γ-PGA/ε-PLL (PP), emerged from the union of γ-PGA and ε-PLL, capitalizing on the ion-based physical interactions [19]. When applied to burn wounds or tracheal mucosa, this dressing efficiently absorbs surrounding tissue fluid, adhering to the wound to create a protective barrier and foster tissue regeneration [20,21]. On this basis, it is considered that single treatment can not completely solve the

* Corresponding authors.
E-mail addresses: wonderluis@sjtu.edu.cn (X. Wang), liangbo@fjmu.edu.cn (B. Liang), jigy_dor@163.com (G. Ji).
[1] These authors contributed equally to this work.

https://doi.org/10.1016/j.cclet.2023.109457
1001-8417/

problem of chronic wounds, our study amalgamates the virtues of anti-inflammatory, antioxidant, and pro-regenerative bioactive drugs to champion diabetic wound healing.

Chlorogenic acid (CGA), a bioactive dietary polyphenol derived from various plants, stands out for its comprehensive biological attributes, including anti-inflammatory, antioxidant, and antibacterial activities [22]. However, the *o*-diphenol hydroxyl group in its molecular structure is easily oxidized, and heat and light can cause the loss of its biological activity, which leads to certain limitations in its wide range of applications [23,24]. Building on this, metallic ions such as Mg^{2+}, Zn^{2+}, Cu^{2+}, and Sr^{2+} are crucial trace elements in the human body. The proliferation and migration of human umbilical vein endothelial cells (HUVECs) and fibroblasts can be improved by the presence of these ions, as evidenced by various studies, and they also stimulate the secretion of angiogenesis-associated factors [25].

In this work, we have developed a MN patch with a strontium polyphenol network structure supported by bioactive CGA-based strontium ions SrC-MPNs@MN-PP (Scheme 1). CGA and strontium ions interact to form strontium polyphenol networks (SrC-MPNs), which form a relatively stable structure. The MNs patches developed using the PP matrix not only retain their structural integrity but also minimize tissue trauma during the delivery of drugs.

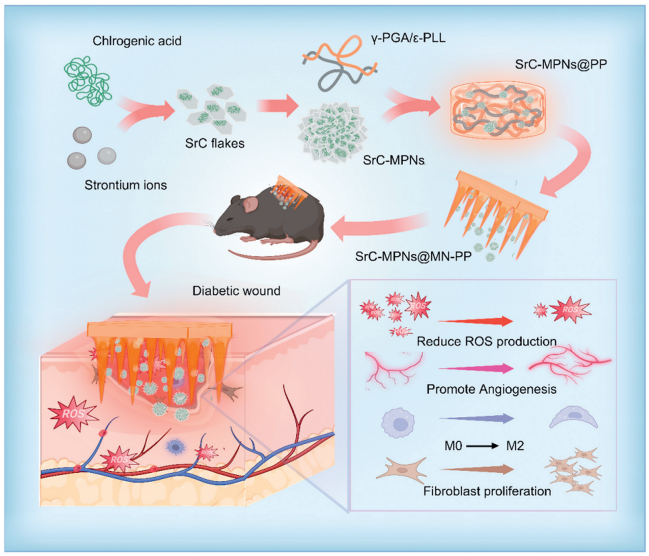

Scheme 1. Schematic of the SrC-MPNs@MN-PP mechanism promoting healing in diabetic wound healing (Image was created with BioRender).

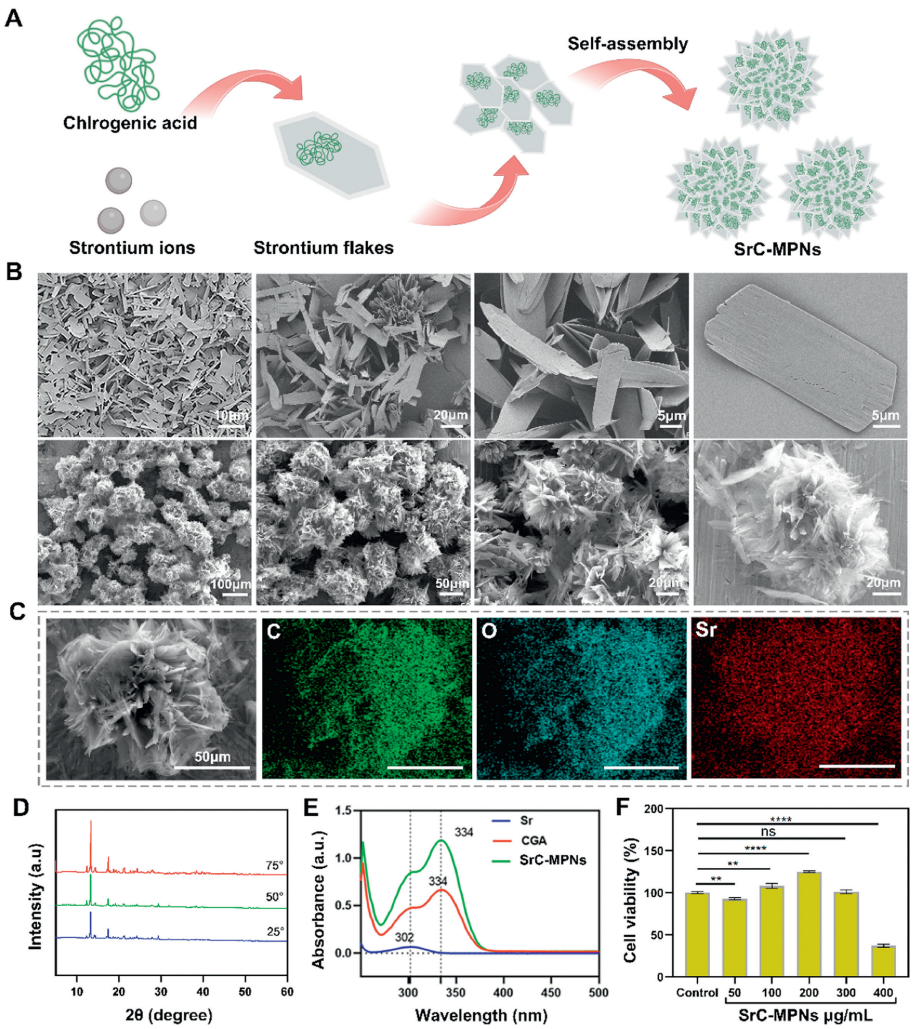

Fig. 1. Synthesis and properties of SrC-MPNs. (A) Schematic representation of SrC-MPN synthesis. (B) SEM image showcasing the self-assembly process of SrC-MPNs structures. (C) Elemental distribution within SrC-MPNs. (D) XRD patterns of SrC-MPNs powder. (E) Concurrent absorption profiles of Sr, CGA, and SrC-MPNs. (F) Cytotoxicity assessment of SrC-MPNs on HUVECs across various concentrations (0, 50, 100, 200, 300, 400 μg/mL) over 48 h. Statistical evaluations were performed with $n = 3$ replicates. All experimental results were expressed as a mean ± standard deviation (SD). $^{**}P < 0.01$, $^{****}P < 0.0001$. ns, not significant.

Earlier research has fused them with metal ions, creating metallic polyphenol network structures. These not only protect the polyphenol drugs but also significantly bolster the healing of diabetic wounds. At pH 7, CGA and strontium ions were self-assembled into SrC-MPNs (Fig. 1A) with biodiversity and porous structure by hydrothermal method. Scanning electron microscopy (SEM) revealed the transition of SrC-MPNs from a singular sheet structure to a consistent spheroidal configuration, averaging around 100 μm in diameter (Fig. 1B). To validate the successful synthesis of SrC-MPNs, element mapping was performed by SEM scanning to determine the composition of SrC-MPNs. Element mapping *via* SEM confirmed the uniform distribution of C, O, and Sr elements within SrC-MPNs (Fig. 1C). To further corroborate the synthesis of SrC-MPNs, powder synthesis was carried out at 25, 50, and 75 °C. Notably, SrC-MPNs exhibited color variations depending on the synthesis temperature (Fig. S1 in Supporting information). X-ray diffraction (XRD) detected characteristic peaks consistently present across the different temperatures, with peak intensities rising alongside temperature, denoting the crystalline integrity of SrC-MPNs (Fig. 1D). Simultaneous absorption peaks for CGA and SrC-MPNs were observed at 334 nm (Fig. 1E and Fig. S2 in Supporting information), and the wave peaks of the two are similar in shape, but the wave peaks are displaced and completely overlapping, suggesting the influence of metal ions. As highlighted in Figs. S3A and B (Supporting information), treating a specific *Staphylococcus aureus* concentration with SrC-MPNs (500, 1000 μg/mL) and sterile water showed a marked reduction in bacterial colony count, affirming the antibacterial properties of SrC-MPNs. It is noteworthy that at concentrations up to 300 μg/mL, SrC-MPNs exhibited no discernible cytotoxicity towards HUVECs (Fig. 1F). As corroborated by previous research, the synthesis methodology employed for SrC-MPNs effectively preserves the biological activity of CGA. Furthermore, SrC-MPNs are distinguished by their unique structural features, stability, and commendable biocompatibility.

For an effective treatment of diabetic wounds, targeted and efficient drug delivery to the affected skin regions is pivotal. Ideally, a dressing with a certain amount of mechanical strength and good solubility is required. The adhesive hydrogel PP, formed through ionic interactions between the negatively charged acidic polymer γ-PGA and the positively charged alkaline polymer ε-PLL, offers such a potential. SrC-MPNs@MN-PP were fabricated by physically cross-linking SrC-MPNs with PP hydrogel using a polydimethylsiloxane (PDMS) microneedle mold, as depicted in Fig. 2A. Fig. 2B showcases the MN mold and the resultant MN patch, highlighting a 10×10 MN array. Mechanical compression tests on MN reveal its adequate mechanical strength to penetrate skin layers (Fig. 2C). SEM imaging depicts the pyramid-like form of SrC-MPNs@MN-PP, emphasizing its uniformity, precise sharpness, and orderliness, ensuring deep skin penetration and sustained drug release for wound healing (Fig. 2D). The moisture-absorbing properties of SrC-MPNs@MN-PP were evaluated by analyzing fluorescence microscopy images of fluorescence-labeled proteins (FITC-BSA) loaded SrC-MPNs@MN-PP at various time intervals under 80% humidity (Fig. 2E). The results indicate a controlled dissolution rate for SrC-MPNs@MN-PP. When applied to mouse wounds, the MN patch dissolved progressively, remaining attached to the wound surface until complete healing. In summation, SrC-MPNs@MN-PP emerges as a potential clinical dressing, offering mechanical resilience, superior moisture retention, effective barrier properties, and precise drug delivery.

The eradication of excess ROS is pivotal for wound healing acceleration, as evidenced by numerous studies [26]. Despite CGA's potent antibacterial, antioxidant, and anti-inflammatory properties, its bioactivity often lacks stability [27]. The microsphere structures of SrC-MPNs, however, are designed to preserve CGA's bioactivity, thus enhancing wound healing potential. Through the employment of 2′,7′-dichlorodihydrofluorescein diacetate (DCFH-DA) as a ROS probe, the levels of ROS in the culture media were assessed by measuring the intensity of green fluorescence, as depicted in Fig. 3A. Pronounced green fluorescence was observed when Raw264.7 was exposed to a medium containing 3 mmol/L H_2O_2. However, when Raw264.7 was cultured with various SrC-MPNs concentrations or extracts of MN-PP and SrC-MPNs@MN-PP (with 100 μg/mL SrC-MPNs). A higher concentration of SrC-MPNs results in a reduction of ROS fluorescence intensity when subjected to the same 3 mmol/L H_2O_2 stimulus. Particularly, culturing in SrC-MPNs@MN-PP (with 100 μg/mL SrC-MPNs) medium demonstrated a marked reduction in ROS fluorescence (Fig. 3B). To quantify the amount of ROS, Raw264.7 cells were stained with the kit and collected for analysis by flow cytometry (Fig. 3C), and the flow cytometry data were quantified (Fig. 3D). Collectively, these findings underscore SrC-MPNs@MN-PP's capability to efficaciously mitigate excess ROS. To further validate the antioxidant potential of SrC-MPNs, fibroblasts were co-cultured with SrC-MPNs and subsequently exposed to 3 mmol/L H_2O_2. An evident positive correlation between SrC-MPNs concentration and fibroblast activity was discerned, corroborated by Fig. 3E. In the end, after verifying the advantage of SrC-MPNs@MN-PP in reducing ROS, the functionality of SrC-MPNs@MN-PP in inducing phenotypic changes in macrophages was further investigated. Raw264.7 cells were co-cultured with extracts from different treatments for 24 h, using an untreated extract as the control. Through reverse transcription quantitative real-time PCR (RT-qPCR), the mRNA expression of the M2 macrophage marker, Arg-1, was gauged. Notably, SrC-MPNs@MN-PP extract treatment significantly augmented Arg-1 expression levels, suggesting an enhanced M2 repolarization post-treatment (Fig. 3H). The specific primer sequences employed

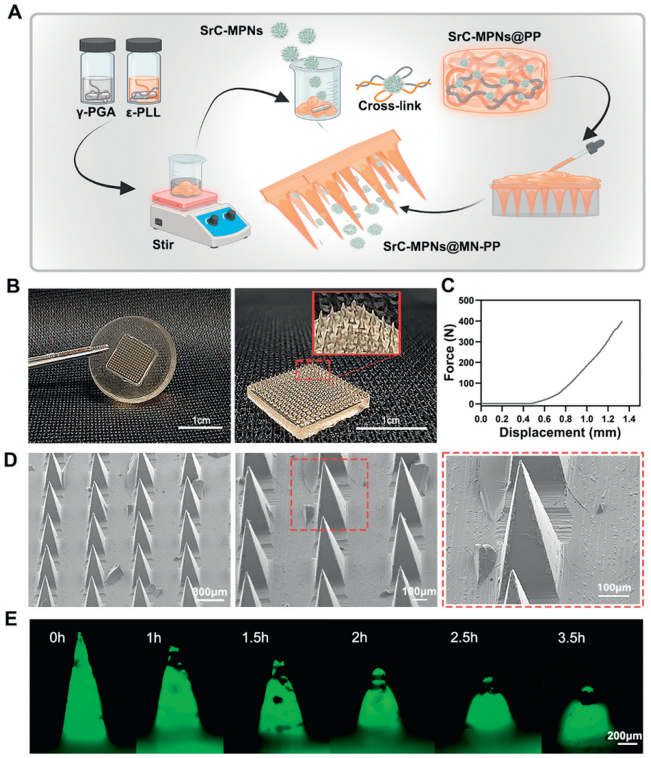

Fig. 2. Synthesis and attributes of SrC-MPNs@MN-PP. (A) Schematic outlining the SrC-MPNs@MN-PP creation process. (B) Frontal, side, and tip views of the SrC-MPNs@MN-PP microneedle structure. (C) Compressive strength analysis of SrC-MPNs@MN-PP. (D) SEM characterization of SrC-MPNs@MN-PP. (E) Time-lapsed fluorescence imagery of SrC-MPNs@MN-PP within an 80% humidity environment at ambient conditions.

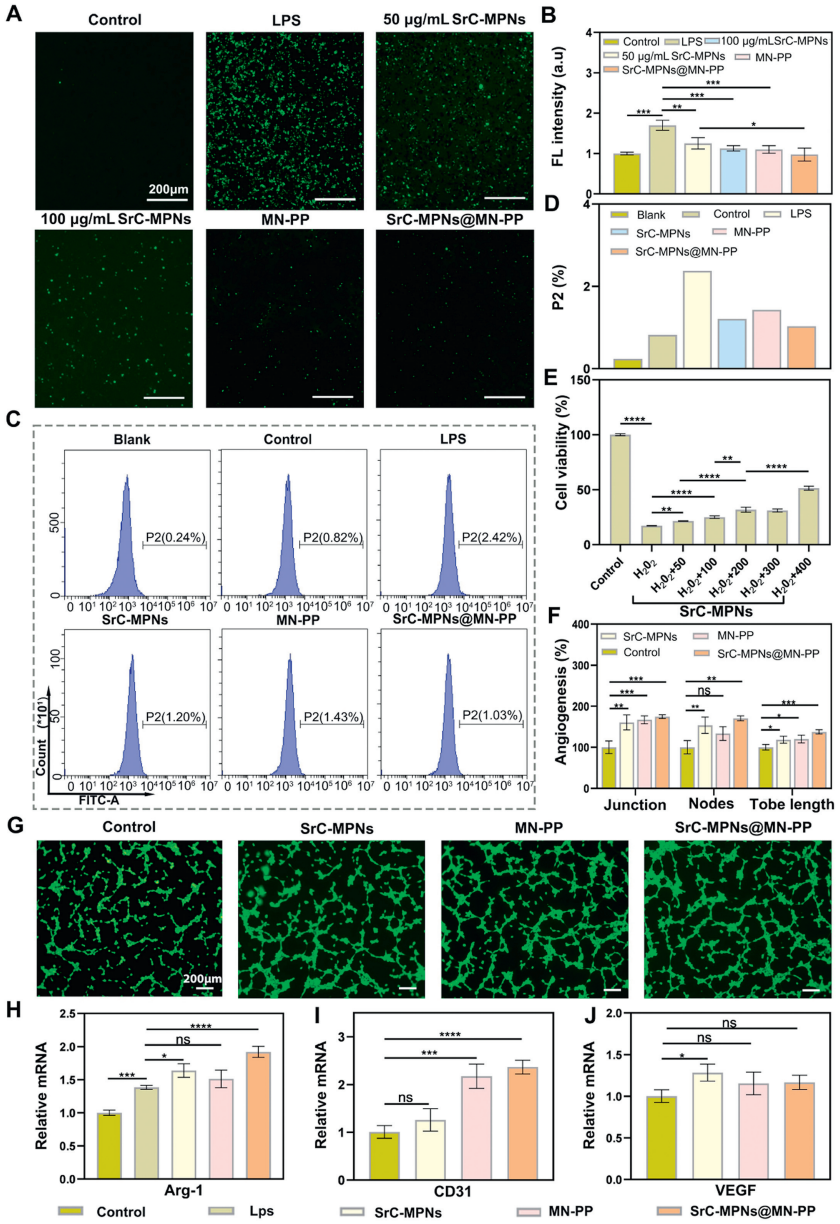

Fig. 3. Antioxidant and angiogenic assessments of SrC-MPNs@MN-PP. (A) After 24 h of treatment with SrC-MPNs (50, 100 μg/mL), LPS, MN-PP extract, SrC-MPNs@MN-PP extract (containing approximately 100 μg/mL SrC-MPNs), or 10% serum medium (control group), ROS levels were assessed in Raw264.7 cells using DCFH-DA staining (green). (B) Quantitative analysis of ROS generation corresponding to (A). (C) Flow cytometric analysis of ROS in Raw264.7 cells across treatments. (D) Statistical analysis of Raw264.7 cells after ROS fluorescence staining, corresponding to image (C). (E) Assessment of human dermal fibroblasts post 24 h co-culture with SrC-MPNs and 30-minute incubation with 3 mmol/L H_2O_2; control group used 10% serum medium. (F) Quantitative metrics on junctions, nodes, and tube lengths across treatments. (G) Representative fluorescence images of HUVECs and different treatment groups after co-culture for 6 h on the cured substrate. (H–J) RT-qPCR analyses of Arg-1, CD31, VEGF post 48-h treatments. Statistical interpretations were drawn from $n = 3$ samples per group; All experimental results were expressed as a mean ± SD. $^{*}P < 0.05$, $^{**}P < 0.01$, $^{***}P < 0.001$, $^{****}P < 0.0001$.

for RT-qPCR are detailed in Fig. S4 (Supporting information). Collectively, these findings reinforce the notion that SrC-MPNs@MN-PP not only mitigates excess ROS but also catalyzes the shift of M0 macrophages towards the pro-healing M2 phenotype, effectively modulating the inflammatory milieu in diabetic wounds.

Angiogenesis plays a pivotal role in diabetic wound healing, with key chemokines such as vascular endothelial growth factor (VEGF) and CD31 driving this process. The *in vitro* angiogenic potential of SrC-MPNs was evaluated using tube formation assays as a surrogate measure for angiogenesis. The results show that SrC-MPNs@MN-PP extract liquid composition tube has the most pronounced effect, as depicted in Fig. 3G. Quantitative metrics like intersection points, nodes, and tube lengths revealed significant enhancement with SrC-MPNs@MN-PP compared to controls (Fig. 3F). To further verify the advantages of SrC-MPNs@MN-PP in promoting tube formation, real-time RT-qPCR was performed, and the mRNA levels of vascular biomarkers (CD31 and VEGF) were detected by RT-qPCR (Figs. 3I and J). The expression of CD31 was markedly higher in the SrC-MPNs@MN-PP extract treatment group when compared to the control group. Furthermore, there was a slight increase in VEGF expression, although it did not reach statistical significance. Collectively, these findings underscore the promising *in vitro* angiogenic capacity of SrC-MPNs@MN-PP, hinting at its potential efficacy *in vivo*.

Ideal medical dressings should not only provide therapeutic benefits but also exhibit superior biocompatibility and minimized cytotoxicity. The biocompatibility and cytotoxicity of SrC-MPNs@MN-PP were evaluated *in vitro*. HUVECs were co-cultured

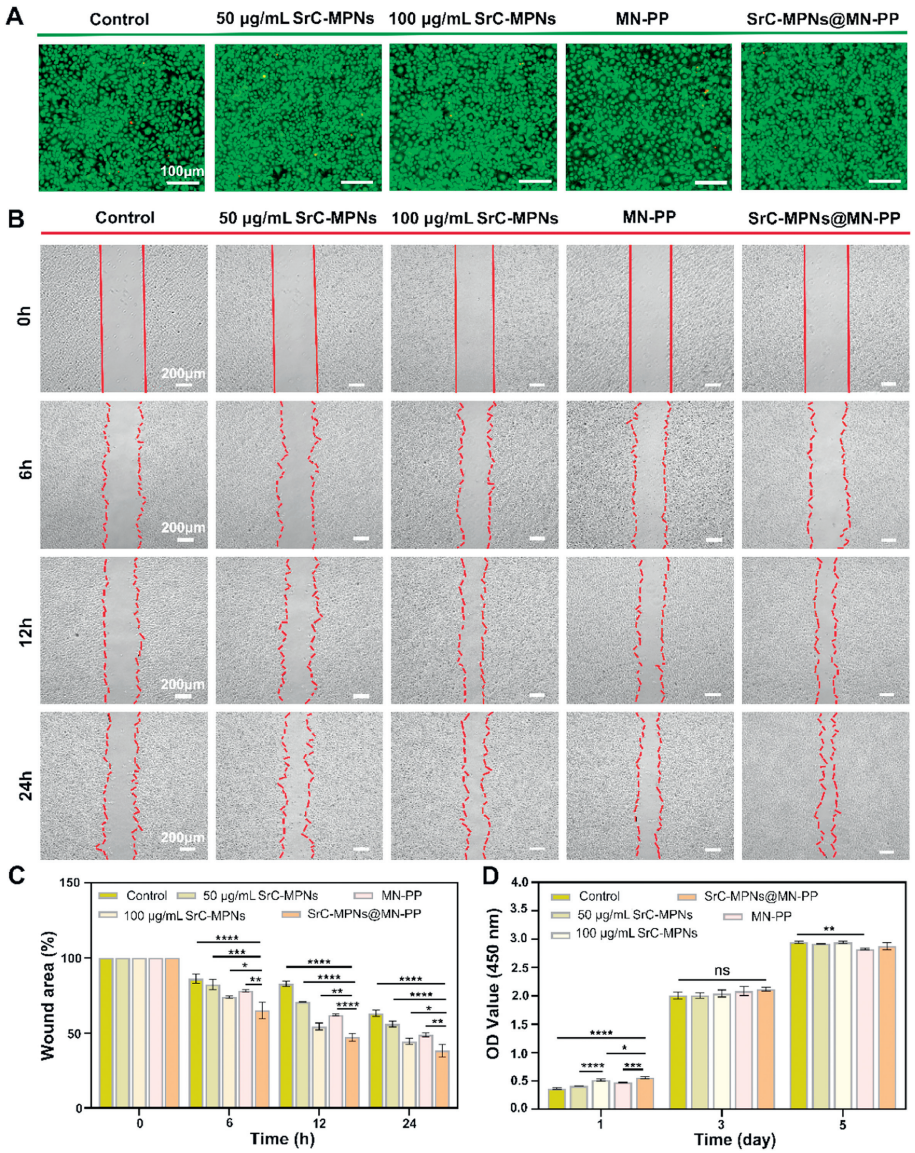

Fig. 4. *In vitro* assessment of biocompatibility, and the proliferative and migratory effects of SrC-MPNs@MN-PP. (A) HUVECs were co-cultured for 48 h with extracts of SrC-MPNs (50, 100 μg/mL), MN-PP, or SrC-MPNs@MN-PP (containing approximately 100 μg/mL SrC-MPNs). A medium supplemented with 10% serum served as the control. Subsequently, cell viability was assessed using specific live/dead stains, with results visualized under fluorescence microscopy. B) Fibroblasts co-cultured with different treatment groups were subjected to a scratch assay to evaluate cellular migration and regeneration. (C) Quantitative analysis of wound closure rates across various treatment groups, corresponding to (B). (D) Proliferative responses of fibroblasts post-treatment were quantified by measuring optical density (OD) values over 1, 3, and 5 days. All experimental results were expressed as a mean ± SD, $n = 3$. $^{*}P < 0.05$, $^{**}P < 0.01$, $^{***}P < 0.001$, $^{****}P < 0.0001$.

with different processing groups. Live/dead cell staining was performed (Fig. 4A) to determine viability. Results confirmed that SrC-MPNs@MN-PP exhibited strong biocompatibility and lacked cytotoxic effects. The cell scratch method was employed to gauge the impact of different processing groups on cell migration and proliferation. Compared to the control group, all treatment groups notably enhanced cell migration and proliferation, with SrC-MPNs@MN-PP showing the most pronounced effects (Figs. 4B and C). In summary, SrC-MPNs@MN-PP has excellent biocompatibility *in vitro* and promotes cell proliferation and migration, which is expected to find applications in the medical industry in the future. The biocompatibility of SrC-MPNs@MN-PP was evaluated by measuring the absorbance optical density (OD) values of fibroblasts at 1, 3, and 5 days using the cell counting kit-8 (CCK-8) assay. The experimental results show that SrC-MPNs@MN-PP exhibit no significant cytotoxicity and good biocompatibility (Fig. 4D).

To evaluate the effectiveness of SrC-MPNs@MN-PP in wound healing, a diabetic mouse model was created with an incision. The experimental procedures were carried out in compliance with the institutional regulations for the care and utilization of laboratory animals and protocols, which were sanctioned by the Animal Care and Use Committee of Shanghai Ninth People's Hospital. After surgery, mice were divided into four groups: control group, SrC-MPNs powder, MN-PP, and SrC-MPNs@MN-PP. Wound progression in different treatment groups was monitored at day 0, 3, 5, 7, 11, 15, and 17 (Fig. 5A). It was observed that the MN patch melted once applied to the wound and remained in place until the wound healed. By day 17, the wounds in the SrC-MPNs@MN-PP group were mostly healed, whereas those in other groups were not fully recovered. The percentage of wound area on different days was quantified (Fig. 5B). While all treated groups showed improved wound healing compared to the control, the SrC-MPNs@MN-PP group was notably more effective.

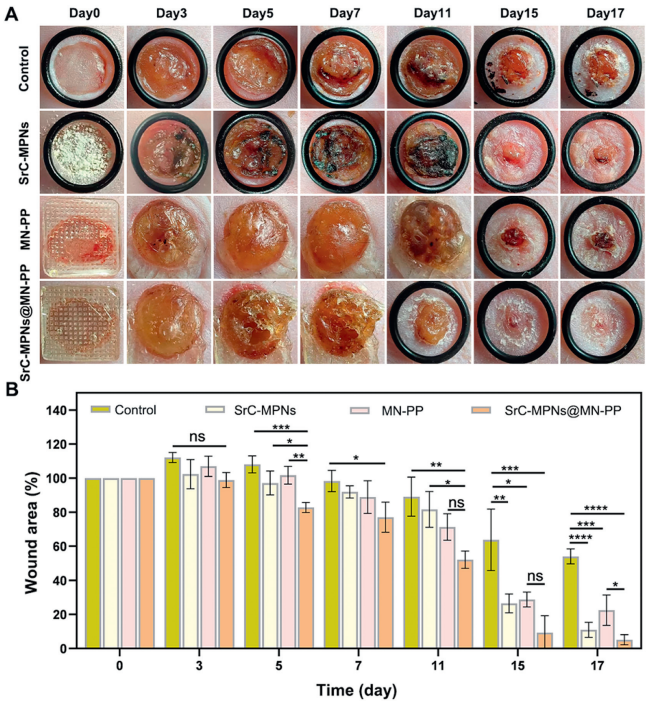

Fig. 5. *In vivo* wound healing promotion in diabetic mice by SrC-MPNs@MN-PP microneedle patches. (A) Diabetic rats were treated with different interventions (SrC-MPNs, MN-PP, SrC-MPNs@MN-PP) applied to the wound surface, while a control group received no treatment. Representative images were captured at 0, 3, 5, 7, 11, 15, and 17 days, respectively. (B) The wound healing rate was assessed for each treatment group, corresponding to the aforementioned images (A). Statistical analysis was conducted with $n = 3$ samples per group. All experimental results were expressed as a mean ± SD. $^{*}P < 0.05$, $^{**}P < 0.01$, $^{***}P < 0.001$, $^{****}P < 0.0001$.

The transition of macrophages from the inflammatory M1 phenotype to the pro-healing M2 phenotype is a critical step in wound healing. The aim of this study was to investigate the potential of SrC-MPNs@MN-PP in modulating the transition of diabetic wounds. Wound tissue samples were collected from various treatment groups, and the expression of macrophage markers CD68, inducible nitric oxide synthase (iNOS), and CD206 was evaluated through immunofluorescence staining. The CD68/iNOS double staining images (Fig. S5A in Supporting information) and the quantification of $CD68^{+}$ $iNOS^{+}$ cell count (Fig. S5B in Supporting information) on day 3 revealed that the treatment with SrC-MPNs powder, MN-PP, and SrC-MPNs@MN-PP led to a significant reduction in M1 polarization, as compared to the control group. The M1 polarization in the control group increased by 2.44-, 1.60-, and 2.87-fold compared to the treatment groups (SrC-MPNs, MN-PP, and SrC-MPNs@MN-PP), respectively. SrC-MPNs is also 1.18-fold higher than SrC-MPNs@MN-PP powder (Fig. S5B). On day 7, the M1 polarization in the control group increased by 2.77-, 1.77- and 3.70-fold compared to the treatment groups, respectively, and SrC-MPNs is also increased 1.34-fold compared with SrC-MPNs@MN-PP powder (Fig. S5B). In addition, on day 17, the M1 polarization in the control group increased by 1.93-, 1.71- and 2.18-fold compared to the treatment groups, respectively. SrC-MPNs is also increased by a factor of 1.34-fold compared to SrC-MPNs@MN-PP powder. In conclusion, while all treatment groups displayed a shift towards a reduction in M1 macrophages, the SrC-MPNs@MN-PP group was the most effective.

After assessing M1 macrophages, our focus shifted to M2 repolarization, which is a critical phase in the process of wound healing. Using CD68/CD206 double staining, the M2 repolarization was assessed (Fig. S6A in Supporting information). By day 3, the SrC-MPNs powder, MN-PP, and SrC-MPNs@MN-PP groups demonstrated increases in M2 repolarization of 2.79-, 3.38-, and 5.90-fold, respectively, compared to the control. Notably, SrC-MPNs@MN-PP exhibited a 2.11-fold increase over the SrC-MPNs powder. On day 7, the M2 repolarization of SrC-MPNs powder, MN-PP and SrC-MPNs@MN-PP group increased by 1.78-, 1.60- and 2.18-fold, respectively, and SrC-MPNs@MN-PP increased by 1.23-fold compared with SrC-MPNs powder (Fig. S6B in Supporting information). On day 17, the enhancement effect of SrC-MPNs powder, MN-PP and SrC-MPNs@MN-PP on repolarization was the same, which was 1.45-, 1.46- and 1.91-fold, respectively, and SrC-MPNs@MN-PP was 1.31-fold higher than that of SrC-MPNs powder (Fig. S6B). In essence, SrC-MPNs@MN-PP not only reduced M1 macrophage polarization but also significantly amplified M2 repolarization, showcasing its potential in promoting wound healing.

To assess tissue regeneration and repair, various staining techniques were utilized in our study. Hematoxylin-eosin staining (H&E) revealed granulation tissue formation and allowed for the measurement of tissue levels, as well as the observation of epithelial repair processes (column 1 of Fig. S7A in Supporting information). By day 17, the SrC-MPNs@MN-PP group exhibited fully formed epithelium, while the control and other treatment groups showed incomplete epithelial healing, as denoted by black arrows. In addition, collagen fibers and muscle fibers were detected and distinguished by Masson tricolor staining by staining collagen fibers in animal tissues blue, muscle fibers red, and cell nuclei blue (Fig. S7A, column 2). SrC-MPNs@MN-PP better enables tissue collagen deposition, promoting wound healing and good tissue remodeling.

Furthermore, immunofluorescence staining was used to assess tissue regeneration, marking cell proliferation and capillaries with CD31 and Ki67, respectively (Fig. S7D in Supporting information). Quantitative analyses demonstrated a substantial increase in capillary density and cell regeneration in the SrC-MPNs powder, MN-PP, and SrC-MPNs@MN-PP groups compared to controls (Figs. S7B and C in Supporting information). The experimental results demonstrate that compared to the control group, the capillary density in SrC-MPNs powder, MN-PP and SrC-MPNs@MN-PP groups increased by 1.20-, 1.19- and 1.70-fold, respectively. The SrC-MPNs@MN-PP group is 1.36-fold that of SrC-MPNs powder. In addition, by quantifying the number of regenerated cells, the SrC-MPNs powder, MN-PP, and SrC-MPNs@MN-PP groups increased by 1.79-, 2.22-, and 2.80-fold, respectively, compared to the control group. The SrC-MPNs@MN-PP group is 1.56-fold more abundant than the SrC-MPNs powder. Collectively, these results signify that SrC-MPNs@MN-PP markedly bolsters *in vivo* tissue regeneration, presenting enhanced wound healing, tissue regeneration, and angiogenesis over control or single treatment methods.

In summary, SrC-MPNs@MN-PP combines the therapeutic power of SrC-MPNs to accelerate wound healing. Key findings include: (i) Effective deep transdermal delivery by SrC-MPNs@MN-PP, ensuring a sustained drug release. (ii) Comprehensive *in vivo* and *in vitro* evaluations revealed the antioxidant attributes of SrC-MPNs@MN-PP, along with its potential to foster cell proliferation, migration, and tissue regeneration. (iii) SrC-MPNs@MN-PP patch has hygroscopic properties, absorbs excess tissue penetrant fluid on the wound surface, and is applied to the wound surface until the wound is healed to isolate the wound from the external environment. Overall, SrC-MPNs@MN-PP presents a promising strategy to expedite the healing of diabetic wounds through its multifunctional therapeutic attributes.

Declaration of competing interest

The authors declare that they have no known competing financial interests or personal relationships that could have appeared to influence the work reported in this paper.

Acknowledgments

This work was financially supported by the National Natural Science Foundation of China (No. 31971271). The Natural Science Foundation of Fujian Province of China (No. 2022J01794). The Science and Technology Plan Project of Quanzhou (No. 2021N033S).

Supplementary materials

Supplementary material associated with this article can be found, in the online version, at doi:10.1016/j.cclet.2023.109457.

References

[1] S. Khosla, P. Samakkarnthai, D.G. Monroe, J.N. Farr, Nat. Rev. Endocrinol. 17 (2021) 685–697.
[2] H. Wu, P. Yang, A. Li, et al., Acta Pharm. Sin. B 13 (2023) 410–424.
[3] R. Mo, H. Zhang, Y. Xu, et al., Adv. Drug Deliv. Rev. 195 (2023) 114753.
[4] S. Noor, R.U. Khan, J. Ahmad, Diabetes Metab. Syndr. 11 (2017) 149–156.
[5] D. Grennan, JAMA 321 (2019) 114.
[6] American Diabetes Association, Diabetes Care 44 (2021) S151–S167.
[7] C. Faselis, A. Katsimardou, K. Imprialos, et al., Curr. Vasc. Pharmacol. 18 (2020) 117–124.
[8] H. Wu, F. Li, W. Shao, J. Gao, D. Ling, ACS Cent. Sci. 5 (2019) 477–485.
[9] J. Holl, C. Kowalewski, Z. Zimek, et al., Cells 10 (2021) 655.
[10] D.G. Armstrong, T.W. Tan, A.J.M. Boulton, S.A. Bus, JAMA 330 (2023) 62–75.
[11] Y. Zhang, C. Xue, Y. Zhang, et al., Chin. Chem. Lett. 35 (2024) 109196.
[12] S.P. Miguel, R.S. Sequeira, A.F. Moreira, et al., Eur. J. Pharm. Biopharm. 139 (2019) 1–22.
[13] E. Yang, W. Hou, K. Liu, et al., Carbohydr. Polym. 291 (2022) 119631.
[14] R.K. Thapa, D.B. Diep, H.H. Tønnesen, Acta Biomater. 103 (2020) 52–67.
[15] M. Yin, X. Wang, Z. Yu, et al., J. Mater. Chem. B 8 (2020) 8395–8404.
[16] M. Yin, J. Wu, M. Deng, et al., ACS Nano 15 (2021) 17842–17853.
[17] P. Wang, J. Wu, H. Yang, et al., Bioact. Mater. 24 (2023) 463–476.
[18] Y. Yang, P. Wang, Y. Gong, et al., Theranostics 13 (2023) 3675–3688.
[19] P. Wang, Y. Pu, Y. Ren, et al., Carbohydr. Polym. 275 (2022) 118692.
[20] C. Hu, H. Ji, Y. Gong, et al., J. Mater. Chem. B (2023) 8666–8678.
[21] Y. Gong, P. Wang, R. Cao, et al., ACS Nano (2023) 22355–22370.
[22] A.K. Singh, R.K. Singla, A.K. Pandey, Curr. Med. Chem. 30 (2023) 3905–3926.
[23] M. Miao, L. Xiang, Adv. Pharm. 87 (2020) 71–88.
[24] H. Lu, Z. Tian, Y. Cui, Z. Liu, X. Ma, Compr. Rev. Food Sci. Food Safety 19 (2020) 3130–3158.
[25] L. Mao, L. Xia, J. Chang, et al., Acta Biomater. 61 (2017) 217–232.
[26] M. Chang, T.T. Nguyen, Acc. Chem. Res. 54 (2021) 1080–1093.
[27] H. Huang, L. Chen, Y. Hou, et al., Colloids Surf. B: Biointerfaces 228 (2023) 113440.